NASA TECHNICAL NOTE

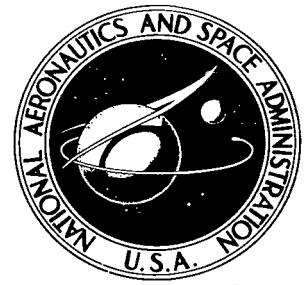

HOT CORROSION OF S-57, A COBALT-BASE ALLOY

Gilbert J. Santoro

Lewis Research Center
Cleveland, Ohio 44135

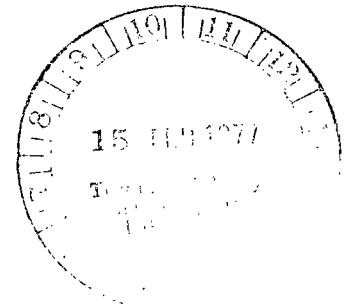

NATIONAL AERONAUTICS AND SPACE ADMINISTRATION • WASHINGTON, D. C. • FEBRUARY 1977

1. Report No.	2. Government Accession No.	3. Recipient's Catalog No.
NASA TN D-8395		

4. Title and Subtitle

HOT CORROSION OF S-57, A COBALT-BASE ALLOY

5. Report Date
February 1977

6. Performing Organization Code

7. Author(s)
Gilbert J. Santoro

8. Performing Organization Report No.
E-8876

9. Performing Organization Name and Address
Lewis Research Center
National Aeronautics and Space Administration
Cleveland, Ohio 44135

10. Work Unit No.
505-01

11. Contract or Grant No.

12. Sponsoring Agency Name and Address
National Aeronautics and Space Administration
Washington, D.C. 20546

13. Type of Report and Period Covered
Technical Note

14. Sponsoring Agency Code

15. Supplementary Notes

16. Abstract

A cobalt-base alloy, S-57, was hot corrosion tested in Mach 0.3 burner rig combustion gases at maximum alloy temperatures of 900° and 1000° C. Various salt concentrations were injected into the burner: 0.5, 2, 5, and 10 ppm synthetic sea salt and 4 ppm sodium sulfate (Na_2SO_4). S-57 underwent accelerated corrosion only under the most severe test conditions, for example, 4 ppm Na_2SO_4 at 900° C. The process of the accelerated corrosion was primarily sulfidation.

17. Key Words (Suggested by Author(s))	18. Distribution Statement
Cobalt alloy Corrosion Hot corrosion S-57	Unclassified - unlimited STAR Category 26

19. Security Classif. (of this report)	20. Security Classif. (of this page)	21. No. of Pages	22. Price*
Unclassified	Unclassified	33	$3.50

* For sale by the National Technical Information Service, Springfield, Virginia 22161

HOT CORROSION OF S-57, A COBALT-BASE ALLOY

by Gilbert J. Santoro

Lewis Research Center

SUMMARY

A cobalt-base alloy, S-57, was subjected to hot corrosion in Mach 0.3 burner rig combustion gases at maximum alloy temperatures of 900° and 1000° C. Various salt concentrations were injected into the burner: 0.5, 2, 5, and 10 ppm synthetic sea salt and 4 ppm sodium sulfate (Na_2SO_4). The extent of corrosion was determined by thickness measurements, and the corrosion process was studied by metallography, X-ray diffraction, scanning electron microscopy, and electron microprobe analysis. While S-57 possessed only moderate oxidation resistance at these temperatures, this alloy resisted significant hot corrosion attack under all but the most severe test conditions, for example, 4 ppm Na_2SO_4 at 900° C. The process of the hot corrosion attack was primarily one of sulfidation.

INTRODUCTION

Hot corrosion can occur in gas turbines in aircraft, in marine power plants, and in land-based power generators. This type of accelerated attack is considered to be due to deposits of sodium sulfate (Na_2SO_4) which increase the alloy oxidation. The Na_2SO_4 can be ingested in the turbine intake air or can be produced by a reaction between sodium chloride (NaCl) ingested in the intake air and sulfur in the fuel. A number of explanations to account for this type of hot corrosion have been published (refs. 1 to 5). An excellent review of the entire field is given in reference 6, while hot corrosion of simple cobalt-base alloys is discussed in detail in reference 7.

Cobalt-base superalloys in general are more hot corrosion resistant than their nickel-base counterparts (ref. 8). There are a number of reasons given to account for this difference. Cobalt-base superalloys achieve high temperature primarily by solid solution and carbide strengthening mechanisms and contain a larger percentage of chromium (20 to 30 wt. %) than nickel-base alloys. Chromium is considered very beneficial in resisting hot corrosion attack. Nickel-base superalloys, on the other hand, achieve

high temperature strength primarily by the precipitation of the γ' phase, nickel aluminum titanium ($Ni_3(Al, Ti)$). In these alloys the chromium content has been lowered in order to raise the γ' solvus temperature to maintain desirable mechanical properties to high temperatures. Further, hot corrosion resistance may also be a function of the sulfide properties of these systems, and the cobalt - cobalt sulfide ($Co-Co_4S_3$) eutectic (877° C) is more refractory than the nickel - nickel sulfide ($Ni-Ni_3S_2$) eutectic (645° C). Finally, the diffusivity of sulfur is lower in cobalt than in nickel (ref. 8).

A wrought cobalt-base alloy, S-57, was recently developed specifically to resist hot corrosion attack by the Centre de Recherches Métallurgiques (ref. 9). The alloy has the nominal composition in weight percent of cobalt-25chromium-10nickel-5tantalum-3aluminum-0.5yttrium (Co-25Cr-10Ni-5Ta-3Al-0.5Y). The chromium and the aluminum were added to provide corrosion resistance to the alloy, the nickel to stabilize the face-centered-cubic matrix, the tantalum to act as a solid solution strengthener, and the yttrium to aid scale adherence and thus to promote corrosion resistance.

In comparison with other alloys, S-57 showed good results in isothermal oxidation tests and in combustion gas hot corrosion tests; for example, S-57 was more resistant than cast X-40 (cobalt-25.5chromium-10.5nickel-7.5tungsten-2iron-1manganese-0.5 carbon (Co-25.5Cr-10.5Ni-7.5W-2Fe-1Mn-0.5C)) (ref. 9). But a systematic study of the hot corrosion resistance of S-57 under simulated turbine engine (burner rig) conditions has not been published. Therefore, the purpose of this study was to provide an evaluation of the hot corrosion of S-57 by using Mach 0.3 burner rig combustion gases (from Jet A-1 fuel) to which various concentrations of synthetic sea salt as well as one concentration of sodium sulfate were added. Specimens were exposed to maximum alloy temperatures of 900° and 1000° C. The extent of the attack was measured, and its nature was studied by metallography, X-ray diffraction, scanning electron microscopy, and electron microprobe analysis.

EXPERIMENTAL PROCEDURE

A 600- by 300- by 1.5-millimeter- (23.6- by 11.8- by 0.59-in.-) thick sheet of S-57 (Co-25Cr-10Ni-5Ta-3Al-0.5Y) was supplied by J. M. Drapier of CRM, Liege, Belgium. The sheet was cut into strips 1.25 by 7.62 centimeters ($\frac{1}{2}$ by 3 in.). The thickness of each strip was measured with a bench micrometer to within ±2 micrometers. The strip specimens were then ultrasonically cleaned in ethyl alcohol, dried, and weighed. One specimen of S-57 per run was loaded into an eight-position circular specimen holder (fig. 1). The other seven positions in the holder were loaded with specimens of other alloys of interest. All specimens were of the same length and width. Each specimen extended 2.54 centimeters (1 in.) into the holder, and 5.08 centimeters (2 in.) were left exposed to the burner flame.

A listing of the burner rig parameters and the specimen temperature profile are given in table I and in figure 2, respectively. The Mach 0.3 burner rig used type A-1 Jet fuel (ASTM D-1655), with a sulfur content of 0.02 to 0.06 weight percent. The specimen temperatures were measured optically, and the measurements were corrected by using the values from calibration runs in which a thermocouple was embedded in the hot zone (2.54 cm from the top) of a similarly shaped dummy specimen. Tests were conducted at two maximum alloy temperatures, 900° and 1000° C. Synthetic sea salt (ASTM D-1141, composition given in table II) was added to the combustion chamber at concentrations of 0.5, 2, 5, and 10 ppm with respect to the combustion air. Runs were also made with 4 ppm sodium sulfate, a concentration containing the sodium equivalent of 5 ppm of synthetic sea salt. Also runs were made without salt injection, that is, with straight oxidation.

In all the runs specimens were exposed to the combustion gas flame for 1 hour and then were cooled for 3 minutes by forced air cooling. Periodically the specimens were removed from the holder and weighed. After 100 cycles (100 hr at the maximum temperature) each test was terminated, and the specimens were weighed, washed in hot running water, dried, and weighed. By this method the amount of accumulated water-removable salt deposit was determined. During the rinsing off of the salt, however, some fine particle scale was also removed. The thickness of the alloy visibly unaffected by the corrosion attack was measured on metallographically prepared cross sections with a microscopic cathetometer at a magnification of 100. These measurements were taken at various points along the specimen midcord, including the hot zone. The exposed specimens were also examined by using standard techniques such as X-ray diffraction, metallography, scanning electron microscopy, and electron microprobe analysis.

RESULTS

Salt Deposition

It is interesting to compare the conditions under which salt was deposited during these tests with thermodynamic predictions. Figure 3 presents concentration isopleths from reference 10. Superimposed on these curves are two points (connected by a line) representing the two conditions used in this program. At 900° C the thermodynamic predictions indicate Na_2SO_4 should not condense when the salt concentration is 0.5 ppm, but should condense at all other concentrations. At 1000° C no Na_2SO_4 should condense at any of the salt concentrations used. Table III lists the accumulated weights of the deposit at the maximum alloy temperatures and salt concentrations used in this program. In comparing the last two columns in table III, one must realize that the deposits were condensed on specimens with a temperature gradient. Thus, at a maximum temperature of

1000° C salt can be expected to deposit at cooler locations on the specimen. Furthermore, the predictions are for the deposition of Na_2SO_4, whereas in practice magnesium and calcium compounds are also expected to condense under all the sea salt conditions listed in table III. Also, during the removal of the deposit some fine particle scale came off, which makes the values in table III somewhat high. Therefore, the most the data can be expected to show is the proper trend. This trend is evident in table III. The trend suggests there is sufficient control of the burner rig parameters to attempt to interpret the hot corrosion process for this alloy.

Amount of Corrosion

After the weight change data were corrected for the weight of compounds deposited, all specimens showed a weight loss, from 1 to 15 milligrams per square centimeter during the 900° C runs and from 4 to 25 milligrams per square centimeter during the 1000° C runs. There was no correlation between this weight change and the concentration of the salt injected into the burner. A more meaningful method for determining the extent of corrosion is to measure the maximum depth of corrosion at various locations on the specimen. Since the temperature gradient is known (fig. 2), the amount of corrosion can be determined as a function of temperature for each salt concentration. These results are presented in figure 4. The data suggest a linear relation between the logarithm of the maximum depth of corrosion and the reciprocal of the absolute temperature. The data were subjected to a least-squares analysis for a linear equation. The coefficients for the slope and intercept for the runs with 0, 0.5, 2, and 5 ppm sea salt were so similar that the data were combined and a least-squares analysis was made on the combined data. The results are presented in table IV and in figure 5. Thus, at the lower temperatures there is a wide separation between the runs with 4 ppm Na_2SO_4 and 10 ppm sea salt, and the other runs fall in between. The significance of the lower temperature results is treated in the DISCUSSION section. The three curves converge at the higher temperatures as expected, since hot corrosion is temperature limited by the dew point of Na_2SO_4.

X-Ray Diffraction

Tables V and VI list the oxide phases detected by X-ray diffraction. Table V presents data from the hot zone of each specimen, and table VI gives the phases detected along the entire exposed length of a single specimen which was run at a maximum temperature of 900° C with 5 ppm sea salt. The oxide phases detected in all the specimens were similar. The predominantly occurring phase was a spinel with a lattice

constant that varied between 8.25×10^{-10} and 8.35×10^{-10} meter (8.25 and 8.35 Å). The lattice parameters published in reference 11 indicate that this spinel could be either nickel chromate ($NiCr_2O_4$) with about 25 percent nickel aluminate ($NiAl_2O_4$) or cobalt chromate ($CoCr_2O_4$) with about 25 percent cobalt aluminate ($CoAl_2O_4$). It is shown in the next section that the spinel probably had the latter composition because the region of the microstructure containing the spinel was very low in nickel.

Microstructure

The microstructure of all the corroded specimens consisted of an oxide scale and an internal corrosion zone (e.g., see fig. 6). It is believed that the oxide scale actually consisted of two layers in all cases. The outer layer was porous and had spalled. The remnants appeared occasionally, as shown in figure 7. The porous layer probably consisted of cobalt oxide (CoO) and chromium sesquioxide (Cr_2O_3) because its Co to Cr ratio was about that of the uncorroded alloy (fig. 8). The dense inner layer of the scale was enriched in Cr and depleted in Ni and was the probable location of the spinels detected by X-ray diffraction. Figures 9(a) to (d) present an example of the distribution of the Co, Cr, and Ni in this region. Another feature of the microstructure was the enrichment of tantalum at the interface between the scale and the internal corrosion zone (e.g., see fig. 9(e)).

The internal corrosion zone consisted of a thick dark structure extending from the scale. This structure became progressively thinner as it approached the unaffected alloy. The dark feature in this zone was primarily an aluminum-rich phase in a cobalt-rich matrix (fig. 10). Sulfur was detected in the raster scan of the hot zone of all specimens exposed at 900° C, with the exception of the specimen run in straight oxidation. The location of the sulfur was near the bottom of the internal corrosion zone (fig. 11). No sulfur was detected in the raster scans from the hot zone of any specimens from the 1000° C runs, with the exception of the specimen exposed to 4 ppm Na_2SO_4.

An exception to this general description of the microstructure of the internal corrosion zone was the hot zone of the specimen from the run with 4 ppm Na_2SO_4 at 900° C (fig. 12(a)). The internal corrosion structure was more globular and had light and dark areas. The dark areas were enriched in aluminum and sulfur (fig. 12(b)), and the light areas were enriched in cobalt (fig. 12(c)).

A feature of the hot zone section of the specimen run at 1000° C with 4 ppm Na_2SO_4 and also of the specimen run at 1000° C with 10 ppm sea salt, was that tantalum enrichment was present not only at the scale - internal-corrosion-zone interface, as in the general case, but also in the internal corrosion zone itself, along with aluminum and sulfur enrichment (e.g., see fig. 13).

A summary of the details of the microstructure just described is presented in figure 14. The structure represented by figure 14(a) applies to the hot zone of specimens exposed to straight oxidation at 900° C and to those exposed to 0, 0.5, 2, and 5 ppm sea salt at 1000° C. Figure 14(b) applies to the 900° C run with 0.5, 2, 5, and 10 ppm sea salt. The only difference between the structures in figures 14(a) and (b) is that the latter contains sulfides. In figure 14(c) the internal corrosion zone has a different structure, which is enriched in sulfur and aluminum. Figures 14(d) and (e) show tantalum enrichment within the internal corrosion zone as well as at the interface between this zone and the dense layer of oxide scale. Figure 14(d) shows sulfur in the microstructure, while figure 14(e) does not.

DISCUSSION

The alloy S-57 did not undergo significant accelerated corrosion under the test conditions of this program, except for the most severe conditions. Figure 5 shows that the extent of attack with 0.5, 2, and 5 ppm synthetic sea salt for 100 hours was indistinguishable from that with straight oxidation in the temperature range from 820° to 1000° C. But the attack at the lower temperatures with Na_2SO_4 was more severe than the attack with sea salt, even with concentrations of sea salt having the same or more sodium content ($\geq$5 ppm sea salt). This phenomenon (Na_2SO_4 causing more corrosion than the equivalent sodium concentration of sea salt) has been observed at this laboratory with other alloys. Such observations raise the question of whether there exists sufficient residence time in the burner rig for the NaCl in the sea salt to convert to Na_2SO_4 (refs. 12 to 14). If there were no NaCl conversion, the lack of accelerated corrosion at low temperatures with 0.5, 2, and 5 ppm sea salt could be attributed to the lack of sufficient Na_2SO_4 deposit to sustain attack. Since there is about 10 weight percent Na_2SO_4 in sea salt (table II), the effective concentrations of Na_2SO_4 in the flame could well be 0.5 ppm and lower, which according to reference 10 would be insufficient for condensation. But this possibility must be dismissed for several reasons. Previous work at this laboratory using 5 ppm sea salt in similar tests resulted in accelerated corrosion in many alloys, for example, B-1900, IN-100, and IN-713C (ref. 15). Thus, 5 ppm sea salt has been sufficient in the past to promote hot corrosion. Furthermore, from table III, the amount of deposit from the 900° C, 5-ppm-sea-salt run was 53.6 milligrams. Only a fraction of this weight can be attributed to the deposition of calcium or magnesium salts (ref. 15). Since the exposed area of the specimen was about 13 square centimeters, the specific deposition averaged about 4 milligrams per square centimeter. Likewise the average specific deposition from the 2-ppm-sea-salt run was about 1 milligram per square centimeter. From experience these amounts of salts ought to be ample to cause hot corrosion.

Of course, if there were complete conversion of the NaCl in the sea salt to Na_2SO_4, the amount of deposition from the 5-ppm-sea-salt run ought to be roughly the same as that from the 4-ppm-Na_2SO_4 run. Since there was considerable deposition during the sea-salt run but not nearly as much as in the Na_2SO_4 equivalent run, some of the NaCl must have been converted but not all. Thus, the curve for 0, 0.5, 2, and 5 ppm sea salt in figure 5 must be interpreted as indicating S-57 is resistant to hot corrosion under the conditions represented by this curve.

The 10-ppm-sea-salt curve in figure 5 is more difficult to understand. A repetition of this run duplicated the original results. Other alloys tested at this laboratory have shown the same behavior. Apparently a sufficiently thick salt deposit can lessen the corrosion. The weight of the deposit on this specimen was 476 milligrams (table III), which gave an average specific deposit weight of about 37 milligrams per square centimeter. Perhaps, when the deposit becomes this thick, the conditions of a half-immersion crucible test are simulated. The results from such tests are reported to be erratic; sometimes a great deal of corrosion is produced and at other times very little (ref. 1).

The role of tantalum in the hot corrosion of cobalt-base alloys has been reported as ranging from neutral (refs. 6 and 16) to beneficial (refs. 17 and 18). In corroded S-57 the interface of the oxide and the internal corrosion zone is enriched with tantalum in the form of the compounds listed in table V: sodium tantalate ($NaTaO_3$), chromium tantalate ($CrTaO_4$), and cobalt tantalate ($CoTa_2O_6$). The presence of $NaTaO_3$ suggests a reaction between tantalum pentoxide and sodium monoxide:

$$Ta_2O_5 + Na_2O \rightleftharpoons 2NaTaO_3$$

Thus, the tantalum may reduce the oxide ion content of the salt and discourage basic fluxing of the scale. In reference 19 the beneficial effect of tantalum on the oxidation of Co-20Cr with 4 to 10 weight percent tantalum was attributed to the formation of $CrTaO_4$ at the scale-alloy interface. It was speculated that the tantalum reduced the oxygen activity at the surface of the alloy and prevented the formation of spall-prone cobalt-containing oxides. This same compound was observed in hot corroded specimens of S-57 and may well play a similar role.

The results of this program lead to the following proposed mechanism for the hot corrosion of S-57: Initially a scale of CoO and Cr_2O_3 forms which spalls upon thermal cycling. The porosity of this scale can be due to either or both of two processes:

(1) Basic fluxing of CoO in localized areas causing the oxide to become detached. More scale is then formed and is also detached by local fluxing. Repetition of this process results in a porous scale (ref. 7).

(2) Vaporization of chromium by the reaction (ref. 20)

$$Cr_2O_3(s) + \frac{3}{2} O_2(g) \rightleftharpoons 2CrO_3(g)$$

The consumption of Cr and the lowering of the oxygen activity by tantalum through the formation of $CrTaO_4$ and $CoTa_2O_6$ allow the creation of an inner spinel scale rich in Co, Cr, and Al, probably $CoCr_2O_4 \cdot 25CoAl_2O_4$. This inner scale is dense and provides the corrosion protection for this alloy. The aluminum content of S-57 is too low to form an external scale under the conditions of these tests. Instead it forms an internal oxide. Sulfur from the Na_2SO_4 deposited on the alloy diffuses through the scale to the inner area of the internal corrosion zone, where the oxygen activity is low enough for the formation of sulfides. The loss of sulfur in the salt causes its oxygen ion activity to increase, which promotes basic fluxing of the protective spinel scale. But the chromium and the tantalum react with the oxygen ion to offset the activity of the salt. Thus,

$$Ta_2O_5 + O^{-2} \rightleftharpoons 2TaO_3^-$$

$$Cr_2O_3 + 2O^{-2} + \frac{3}{2} O_2 \rightleftharpoons 2CrO_4^{-2}$$

Under the most severe corrosion conditions, low temperatures and 4 ppm Na_2SO_4, the amount of sulfidation increases and causes the internal corrodents to conglomerate into globules. These globules may be the result of liquid phases consisting of low-temperature eutectics of Co and Ni with their sulfides (ref. 21). The sulfides are preferentially oxidized and release sulfur for further diffusion into the alloy; they thereby extend the depth of the internal corrosion zone (ref. 22).

In the hot zone of specimens from the 1000° C, 10-ppm-sea-salt run and the 1000° C, 4-ppm-Na_2SO_4 run tantalum enrichment was observed in the internal corrosion zone. In the former no sulfur was observed, while it was present in the latter. An explanation as to why a tantalum-enriched phase should appear only under these two conditions will require further investigation.

CONCLUSIONS

From the results generated by an investigation of the cobalt-base alloy S-57 in a Mach 0.3 burner rig at various temperatures and salt concentrations the following major conclusions can be drawn:

1. S-57 does not undergo significant accelerated corrosion attack except under very severe test conditions.

2. The process of the accelerated corrosion is primarily sulfidation. Sulfides formed beneath the scale are preferentially oxidized and release sulfur for further diffusion into the alloy.

3. The presence of chromium and tantalum reduces the basic fluxing of the protective oxide scale.

4. The protective scale is essentially a cobalt, chromium, aluminum spinel, probably cobalt chromate · cobalt aluminate ($CoCr_2O_4 \cdot 25CoAl_2O_4$).

Lewis Research Center,
National Aeronautics and Space Administration,
Cleveland, Ohio, September 22, 1976,
505-01.

REFERENCES

1. Simons, E. L.; Browning, G. V.; and Liebhafsky, H. A.: Sodium Sulfate in Gas Turbines. Corrosion, vol. 11, no. 12, 1955, pp. 17-25.

2. Seybolt, A. U.: Contribution to the Study of Hot Corrosion. Trans. Metall. Soc., AIME, vol. 242, no. 9, Sept. 1968, pp. 1955-1961.

3. Bernstein, N. S.; and DeCrescente, M. A.: The Relationship Between Compounds of Sodium and Sulfur and Sulfidation. Trans. Metall. Soc., AIME, vol. 245, no. 9, Sept. 1969, pp. 1947-1952.

4. Goebel, J. A.; and Pettit, F. S.: Na_2SO_4-Induced Accelerated Oxidation (Hot Corrosion) of Nickel. Metall. Trans., vol. 1, no. 7, July 1970, pp. 1943-1954.

5. Goebel, J. A.; and Pettit, F. S.: The Influence of Sulfides on the Oxidation Behavior of Nickel-Base Alloys. Metall. Trans., vol. 1, no. 12, Dec. 1970, pp. 3421-3429.

6. Stringer, J.: Hot Corrosion in Gas Turbines. MCIC-72-08, Metals and Ceramics Information Center. (AD-745474), 1972.

7. Goebel, J. A.; and Pettit, F. S.: Hot Corrosion of Cobalt-Base Alloys. PWA-5035, Pratt & Whitney Aircraft, 1974.

8. Beltran, A. M.; and Shores, D. A.: Hot Corrosion. The Superalloys. Chester T. Sims and William C. Hagel, eds., ch. 11, John Wiley & Sons, 1974, pp. 317-339.

9. Davin, A.; Coutsouradis, D.; and Habraken, L.: Development and Properties of Cobalt-Base Alloys with Improved Hot-Corrosion Resistance. Cobalt, no. 57, Dec. 1972, pp. 175-181.

10. Kohl, F. J.; Stearns, C. A.; and Fryburg, G. C.: Sodium Sulfate: Vaporization Thermodynamics and Role in Corrosion Flames. Metal-Slag-Gas Reactions and Processes. Z. A. Foroulis and W. W. Smeltzer, eds., The Electrochem. Soc., 1975, pp. 649-674.

11. Zaplatynsky, Isidor: Thermal Expansion of Some Nickel and Cobalt Spinels and Their Solid Solutions. NASA TN D-6174, 1971.

12. Condé, J. F. G.: What Are the Separate and Interacting Roles of Sulfur, Sodium and Chloride in Hot Corrosion? High Temperature Corrosion of Aerospace Alloys. J. Stringer, R. I. Jaffee, and T. F. Kearns, eds., AGARD-CP-120, 1972, pp. 203-219.

13. Condé, J. F. G.; and Wareham, B. A.: Aspects of the Mechanism of Hot Corrosion in Marine Gas Turbines. Proceedings of 1974 Gas Turbine Materials in the Marine Environment Conference. J. W. Fairbanks and I. Machlin, eds., MCIC-75-27, Metals and Ceramics Information Center, 1975, pp. 73-92.

14. Fryxell, R. E.; and Bessen, I. I.: Coating Life Assessment in Gas Turbines Operated for Ship Propulsion. Proceedings of 1974 Gas Turbine Materials in the Marine Environment Conference. J. W. Fairbanks and I. Machlin, eds., MCIC-75-27, Metals and Ceramics Information Center, 1975, pp. 259-276.

15. Santoro, Gilbert: Hot Corrosion of Aluminide Coated Superalloys in Support of an ASTM Round Robin Program. NASA TM X-71734, 1975.

16. Goebel, J. A.; and Pettit, F. S.: Hot Corrosion of Cobalt Alloys. PWA-5379, Pratt & Whitney Aircraft, 1975; also ARL-TR-75-0235.

17. Wright, Ian G.; Wilcox, Ben A.; and Jaffee, Robert I.: Oxidation and Hot Corrosion of Ni-Cr and Co-Cr Base Alloys Containing Rare Earth Oxide Dispersions. Battelle Columbus Lab. (AD-A011379), 1975.

18. Drapier, J. M.; et al.: Obtention of Improved Tensile Properties and Hot-Corrosion Resistance in Cobalt-Base Superalloys. CRM-38, Centre de Recherches Metallurgique (Belgium), 1974, pp. 39-57.

19. Irving, G. N.; Stringer, J.; and Whittle, D. P.: The Oxidation of Co-20% Cr Base Alloys Containing Nb or Ta. Corrosion Sci., vol. 15, 1975, pp. 337-344.

20. Stearns, Carl A.; Kohl, Fred J.; and Fryburg, George C.: Oxidative Vaporization Kinetics of Cr_2O_3 in Oxygen from 1000° to 1300° C. J. Electrochem. Soc., vol. 121, no. 7, July 1974, pp. 945-951.

21. Goebel, J. A.; Felten, E. J.; and Pettit, F. S.: Hot Corrosion Mechanisms for Nickel and Cobalt Base Alloys. Proceedings of 1974 Gas Turbine Materials in

the Marine Environment Conference. J. W. Fairbanks and I. Machlin, eds., MCIC-75-27, Metals and Ceramics Information Center, MCIC-75-27, July 1974.

22. Seybolt, A. U.; and Beltram. A.: High Temperature Sulfur-Oxygen Corrosion of Nickel and Cobalt. Hot Corrosion Problems Associated with Gas Turbines. STP-421, Am. Soc. Testing Mater., 1967, pp. 21-27.

TABLE I. - BURNER RIG TEST PARAMETERS

Burner type	Pratt & Whitney
Mach number	0.3
Fuel	Type A-1, ASTM D-1655
Fuel sulfur content, wt. %	0.02 to 0.06
Air-fuel ratio	
At 900° C	20
At 1000° C	16
Pressure, atm	1
Salt concentration, ppm	
Synthetic sea salt	0, 0.5, 2, 5, or 10
Na_2SO_4	4
Maximum alloy temperature (see fig. 2), °C	900 or 1000
Total time at temperature, hr	100
Cycle	
Time at temperature, hr	1
Forced air cooling time, min	3
Speed of rotation, rpm	300

TABLE II. - SYNTHETIC SEA SALT COMPOSITION

[ASTM D-1141-52, sec. 4.]

Salt	Concentration, wt. %
Sodium chloride	58.490
Magnesium chloride, hexahydrate	26.460
Sodium sulfate	9.750
Calcium chloride	2.765
Potassium chloride	1.645
Sodium bicarbonate	.477
Potassium bromide	.238
Boric acid	.071
Strontium chloride, hexahydrate	.095
Sodium fluoride	.007

TABLE III. - CUMULATIVE WEIGHT OF WATER-REMOVED DEPOSIT

Maximum alloy temperature, °C	Salt	Salt concentration in air, ppm	Weight of deposit, mg (a)	Na_2SO_4 state from ref. 10
900	Sea salt	0.5	1.2	Vapor
	Sea salt	2	12.0	Condensed
	Sea salt	5	53.6	Condensed
	Na_2SO_4	[b]4	169.4	Condensed
	Sea salt	10	476.0	Condensed
1000	Sea salt	0.5	0.2	Vapor
	Sea salt	2	.1	↓
	Sea salt	5	[c]33.6	
	Na_2SO_4	[b]4	[c]32.2	
	Sea salt	10	[c]46.0	

[a]Weights are somewhat high since some loose scale was also lost during process of removing deposit.

[b]4 ppm Na_2SO_4 has Na equivalent of 5 ppm synthetic sea salt.

[c]Value reflects fact that specimens had temperature gradients allowing salt deposition at cooler locations.

TABLE IV. - LEAST-SQUARES ANALYSIS OF S-57 CORROSION DATA

[Equation for analysis, $Y = a_1 + a_2X$, where Y is log of maximum depth of penetration, in μm, and X is reciprocal of temperature, $1/T$, K^{-1}.]

Salt	Salt concentration in air, ppm	Intercept, a_1	Slope, a_2	Correlation coefficient	Standard error of estimate
None	---	6.788	-0.592×10^4	-0.94	$\pm8.2\times10^{-2}$
Sea salt	0.5	6.540	-0.556×10^4	-0.89	$\pm12.0\times10^{-2}$
	2	5.311	-.418	-.92	±7.2
	5	6.026	-.500	-.84	±12.8
	0, 0.5, 2, 5	6.160	-.516	-.88	±8.0
	10	8.956	-.858	-.99	±5.9
Na_2SO_4	4	3.972	-0.237×10^4	-0.61	$\pm12.4\times10^{-2}$

TABLE V. - OXIDE PHASES IN HOT ZONE OF EACH SPECIMEN

DETECTED BY X-RAY DIFFRACTION

[Pattern from area exposed to maximum temperature.]

Salt	Salt concentration in air, ppm	Maximum alloy temperature, ^{o}C	
		900	1000
		Oxide phase[a]	
None	----	Spinel, 8.35×10^{-10} m (8.35 Å) Cr_2O_3 [b]$CrTaO_4$	Cr_2O_3 Spinel, 8.25×10^{-10} m (8.25 Å) $CoTa_2O_6$
Sea salt	0.5	Spinel, 8.25×10^{-10} m (8.25 Å) Cr_2O_3 [b]$CrTaO_4$ [c]CoO	Spinel, 8.30×10^{-10} m (8.30 Å) Cr_2O_3 [b]$CrTaO_4$
	2	$NaTaO_3$ CoO Spinel, 8.25×10^{-10} m (8.25 Å)	Spinel, 8.25×10^{-10} m (8.25 Å) Cr_2O_3
	5	Spinel, 8.25×10^{-10} m (8.25 Å) $NaTaO_3$ Cr_2O_3	Cr_2O_3 Spinel, 8.15×10^{-10} m (8.15 Å) [c]$CrTaO_4$
	10	Spinel, 8.30×10^{-10} m (8.30 Å) $NaTaO_3$ Cr_2O_3 [b]$CrTaO_4$	Spinel, 8.35×10^{-10} m (8.35 Å) CoO Cr_2O_3
Na_2SO_4	4	Spinel, 8.30×10^{-10} m (8.30 Å) $NaTaO_3$ Cr_2O_3	Spinel, 8.25×10^{-10} m $NaTaO_3$

[a]Phases listed in order of decreasing line intensity.

[b]Very weak pattern.

[c]Insufficient lines for positive identification.

TABLE VI. - OXIDE PHASES ALONG LENGTH OF SPECIMEN

DETECTED BY X-RAY DIFFRACTION

[Specimen exposed at 900° C with 5 ppm sea salt.]

Distance from top of specimen, cm (in.)	Temperature, °C	Oxide phase
0-1.27(1/2)	860-890	Spinel, 8.25×10^{-10} m (8.25 Å)
1.27(1/2)-2.54(1)	890-900	Spinel, 8.25×10^{-10} m (8.25 Å) $NaTaO_3$
2.54(1)-3.81(1 1/2)	900-850	Spinel, 8.25×10^{-10} m (8.25 Å) Cr_2O_3 $NaTaO_3$
3.81(1 1/2)-5.08(2)	850-<810	Spinel[a] CoO[a]

[a]Insufficient lines for positive identification.

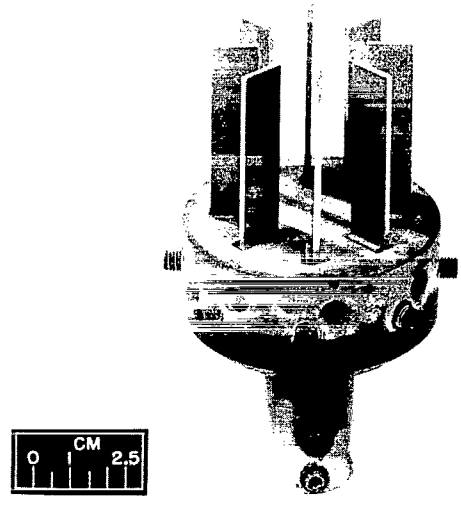

C-76-725

Figure 1. - Burner rig specimen holder with full complement of eight specimens.

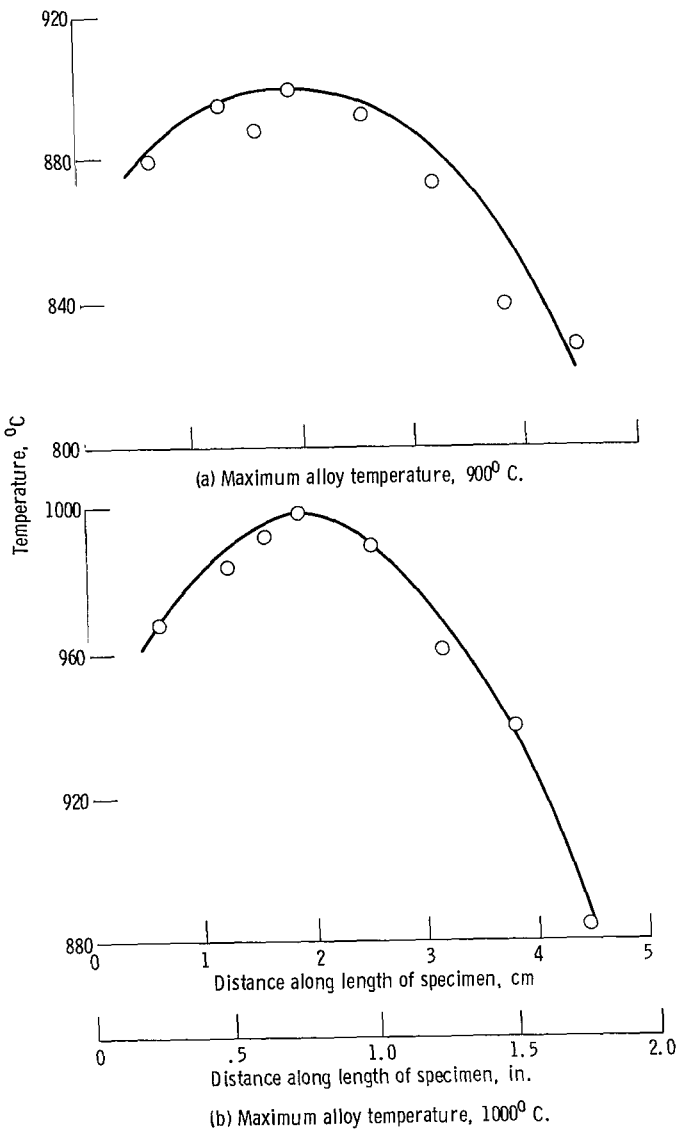

Figure 2. - Temperature profiles. Top of calibration specimen at zero centimeter.

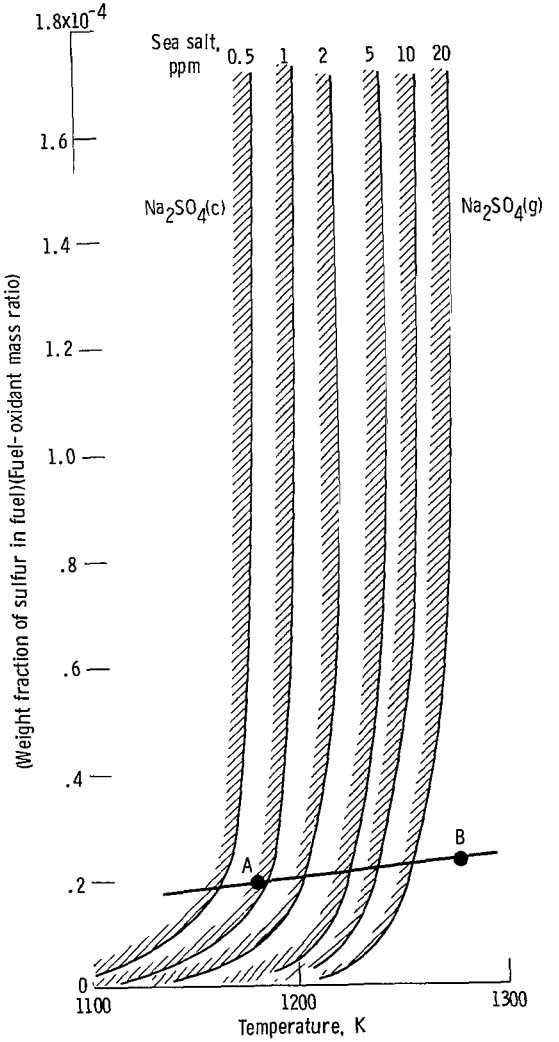

Figure 3. - Condensation temperatures as function of sulfur content and sea-salt concentration from reference 10. Burner rig flame fuel, Jet A ($CH_{1.9185}$) + sulfur; oxidant, air (1 wt. % water) + sea salt; inlet temperature, 298 K; pressure, 1.0 atmosphere. Conditions of this program are denoted by points A and B.

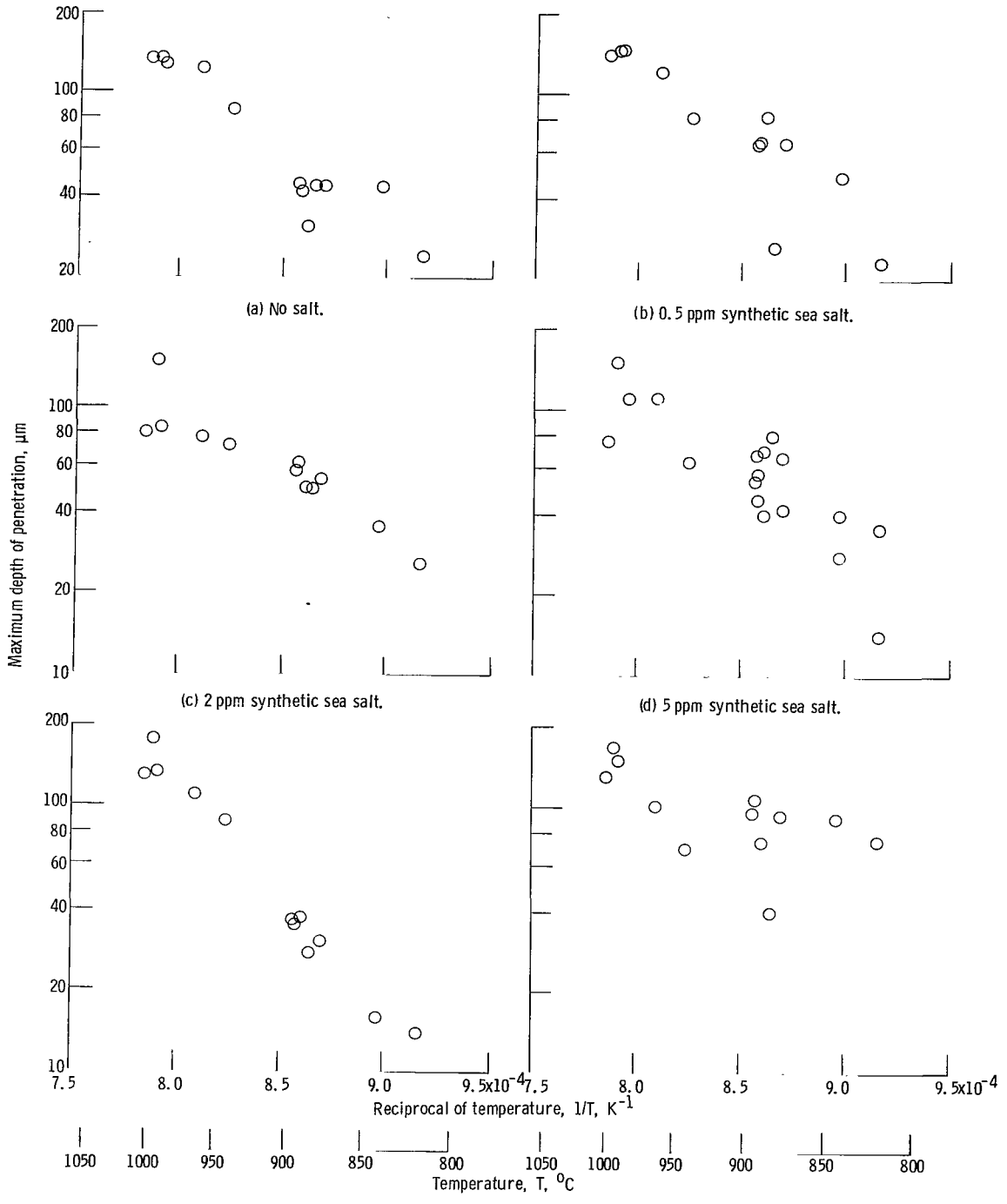

Figure 4. - Extent of corrosion of S-57 after 100 hours in Mach 0.3 burner rig.

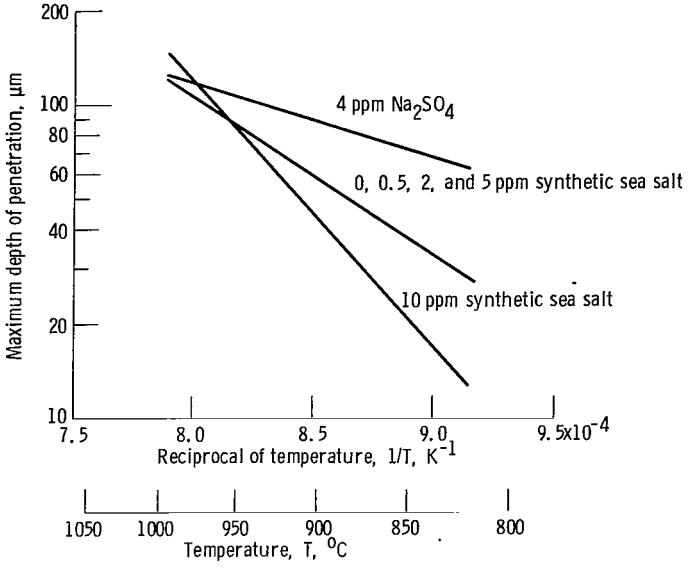

Figure 5. - Least-squares analysis of corrosion data of S-57.

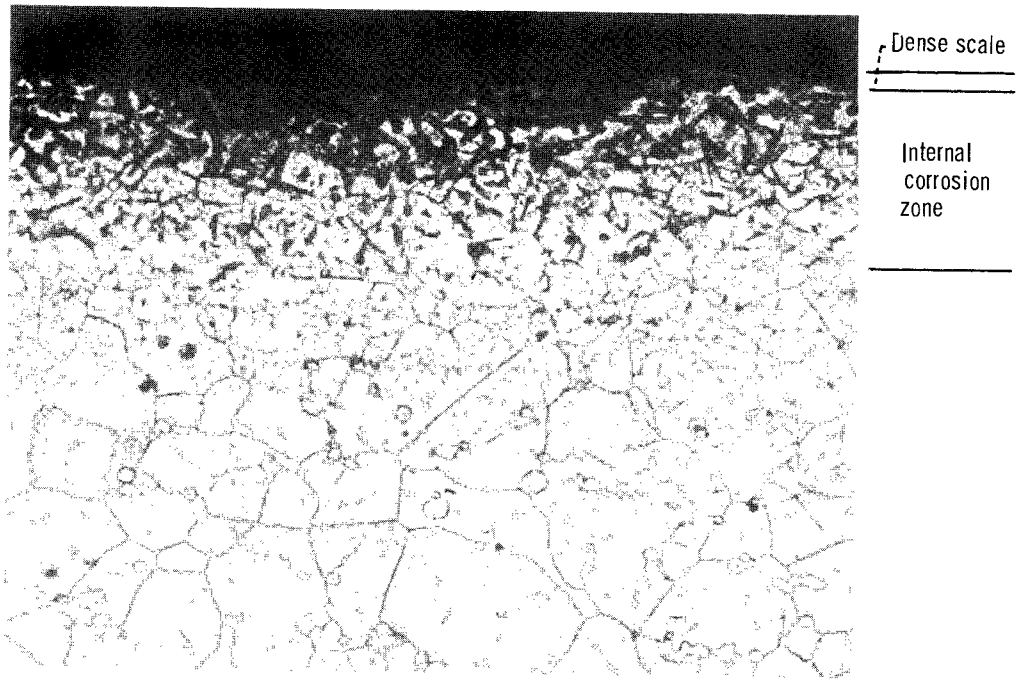

(a) Corroded at 900° C.

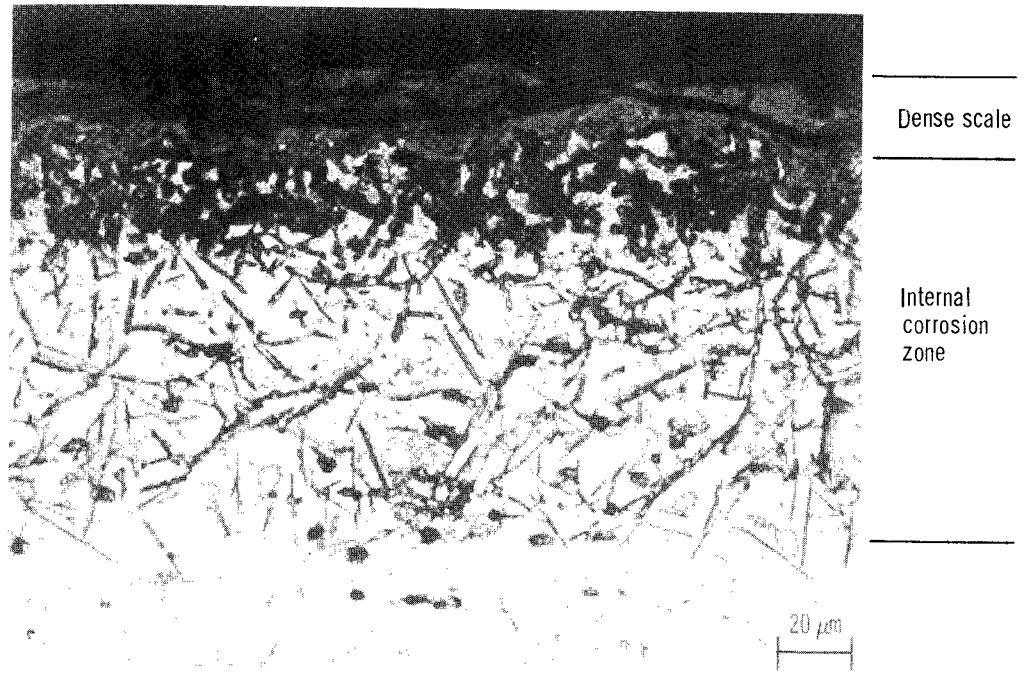

(b) Corroded at 1000° C.

Figure 6. - Typical microstructures of corroded S-57 showing scale and internal corrosion zone. No salt added.

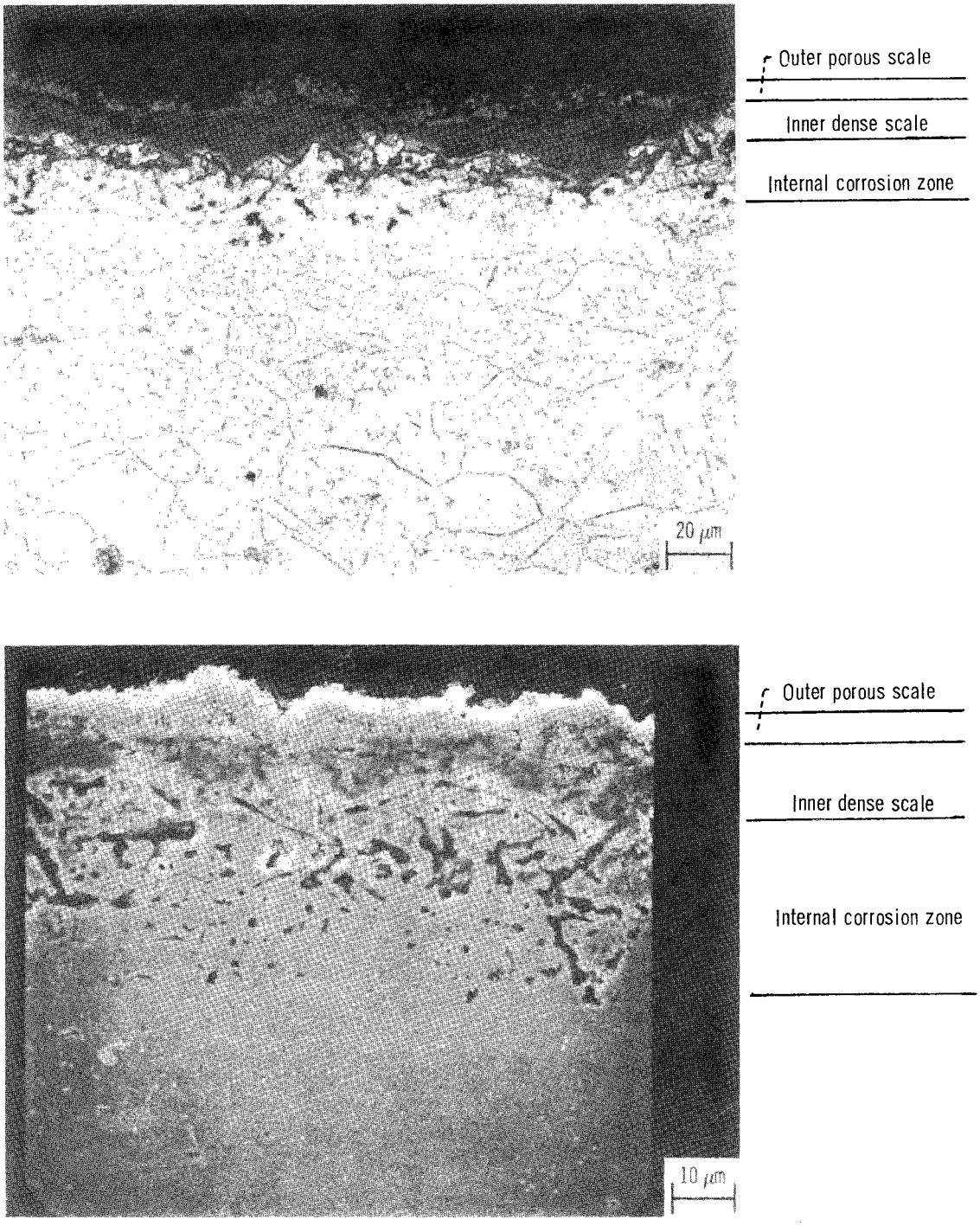

Figure 7. - Microstructures of outer porous scale. Outer scale usually spalled, and only dense inner scale was left. Corroded at 900° C with 5 ppm sea salt.

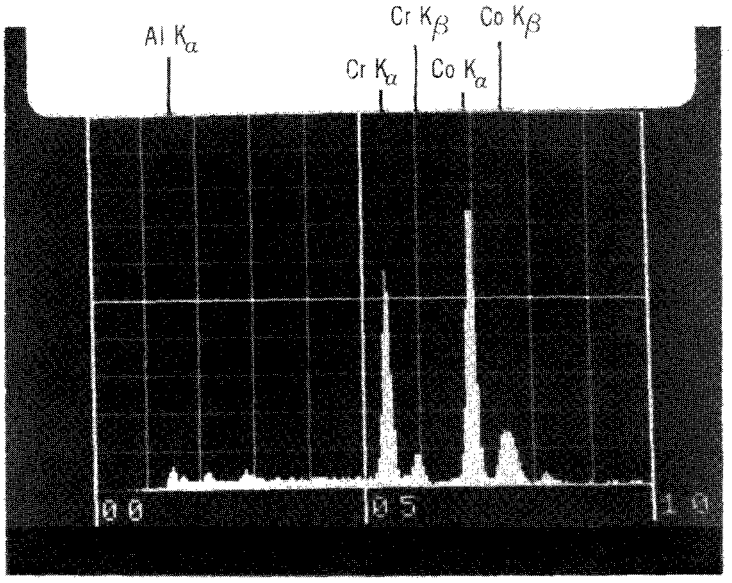

(a) As-received alloy. X3000.

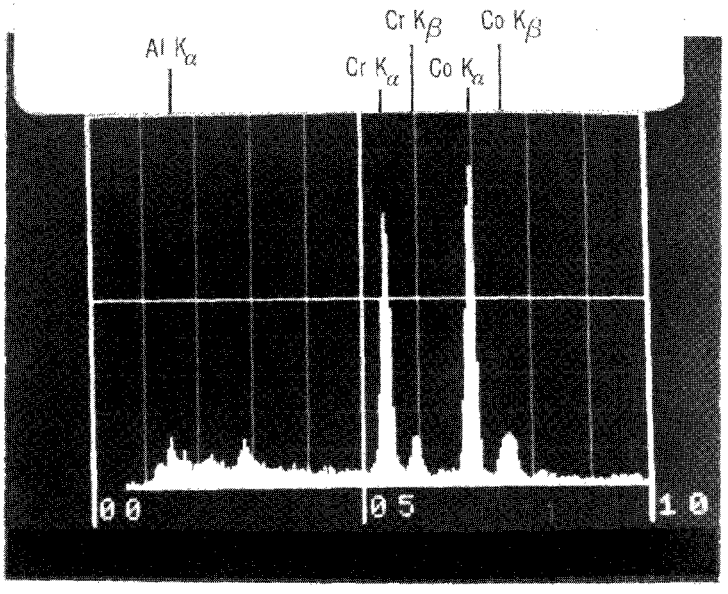

(b) Outer porous scale of alloy corroded at 900° C with 10 ppm sea salt. X30 000.

Figure 8. - Energy dispersive spectrums showing cobalt-chromium ratio.

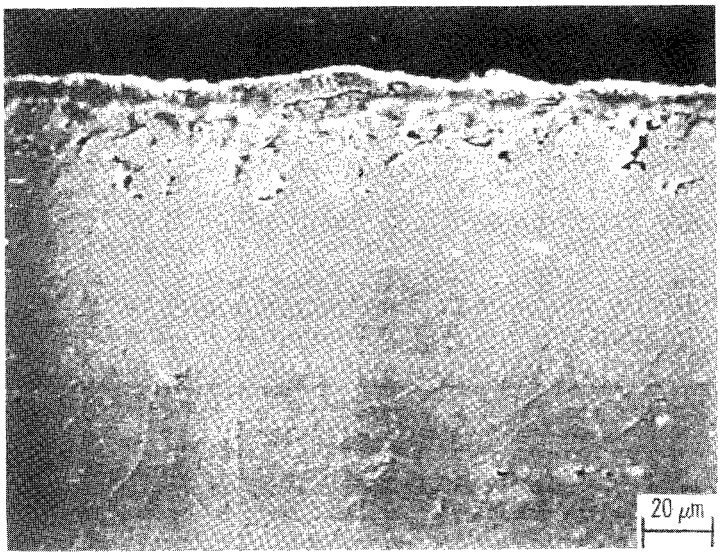

(a) Secondary electron image.

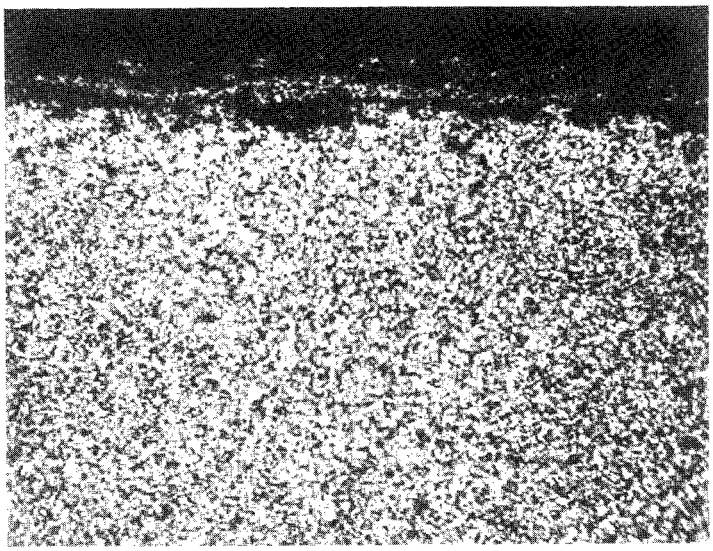

(b) Cobalt K_α raster scan.

Figure 9. - Secondary electron image and raster scans showing distribution of elements in S-57 corroded at 900° C with 10 ppm sea salt.

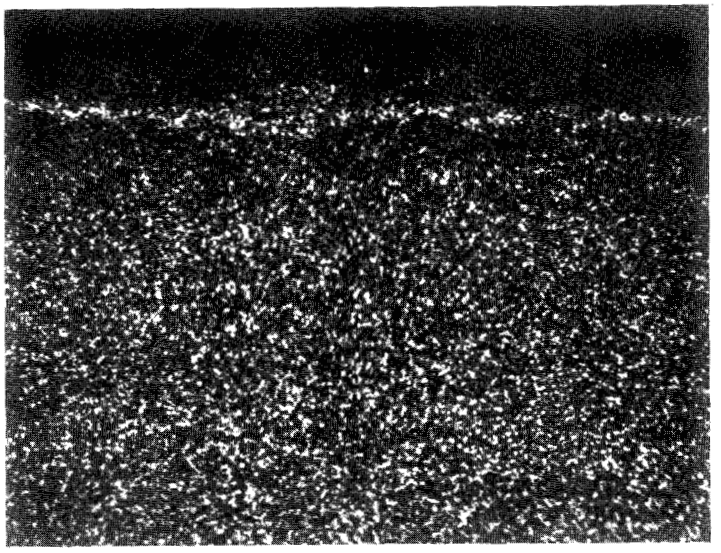

(c) Chromium K_α raster scan; dense scale enriched in chromium.

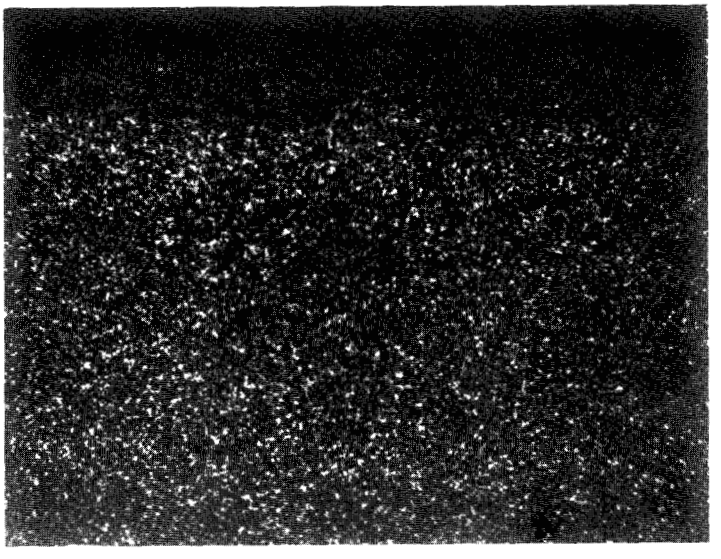

(d) Nickel K_α raster scan; dense scale depleted in nickel.

Figure 9. - Continued.

(e) Tantalum M_α raster scan; interface of scale and internal corrosion zone enriched in tantalum.

Figure 9. - Concluded.

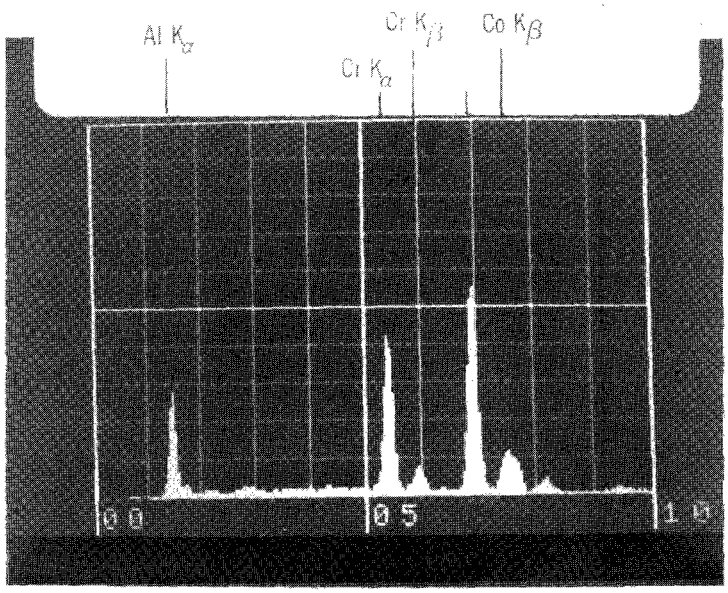

(a) Corroded at 1000° C with no salt; internal corrosion particles just beneath scale.

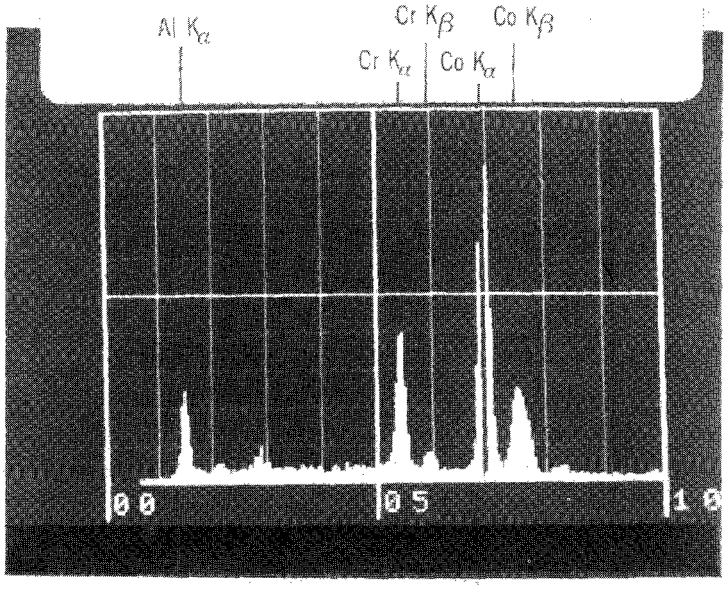

(b) Corroded at 900° C with 10 ppm sea salt; internal corrosion particles just beneath scale.

Figure 10. - Energy dispersive spectrums of internal corrosion zone of S-57 corroded at 1000° C with no salt or at 900° C with 10 ppm sea salt. X30 000.

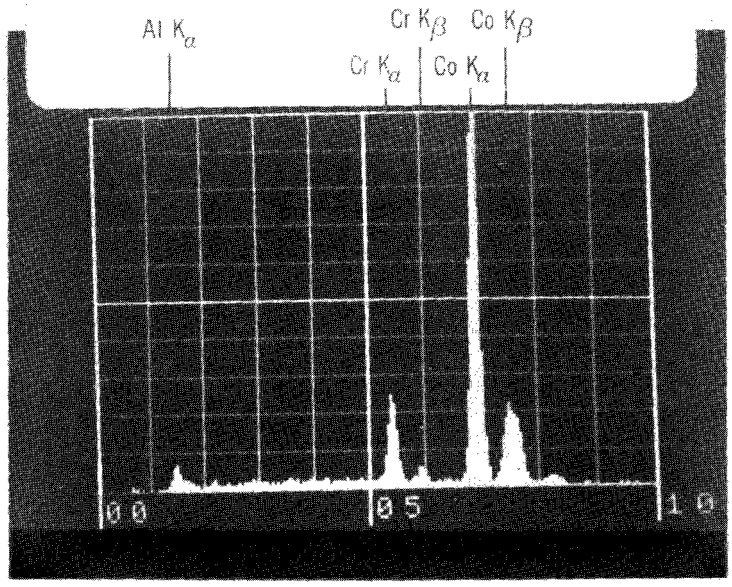

(c) Corroded at 1000° C with no salt; area between corrosion particles.

Figure 10. - Concluded.

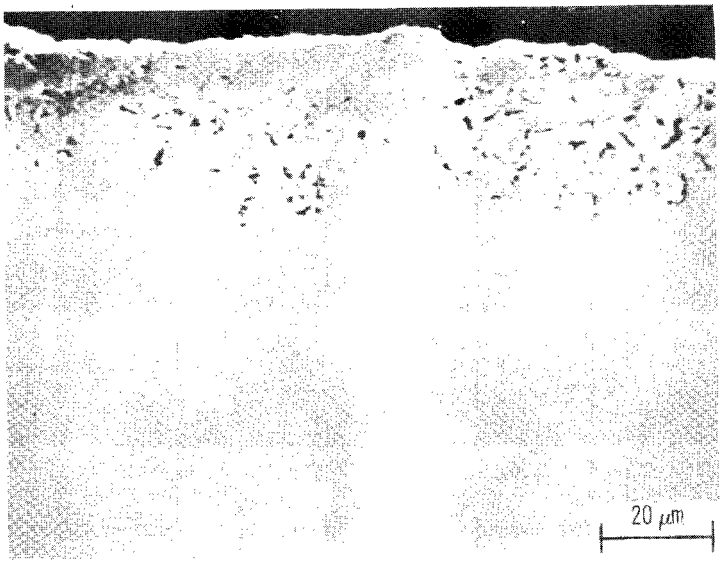

(a) Secondary electron image.

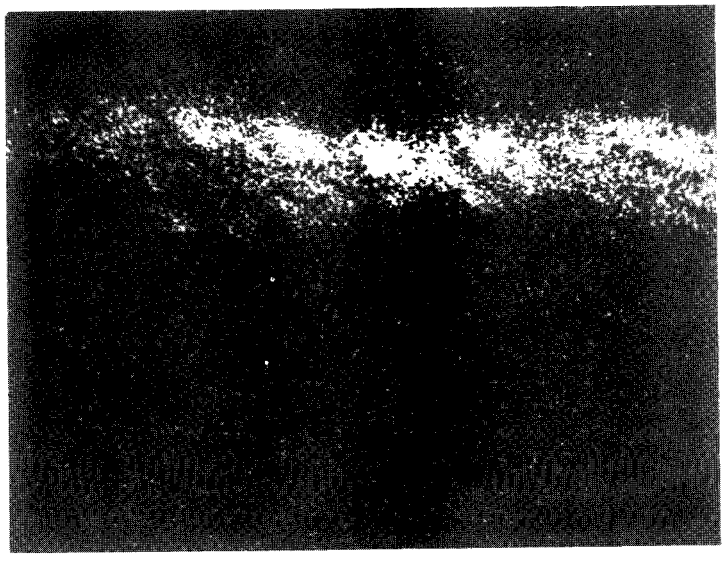

(b) Sulfur K_α raster scan.

Figure 11. - Secondary electron image and raster scan showing location of sulfur in S-57 corroded at 900° C with 5 ppm sea salt.

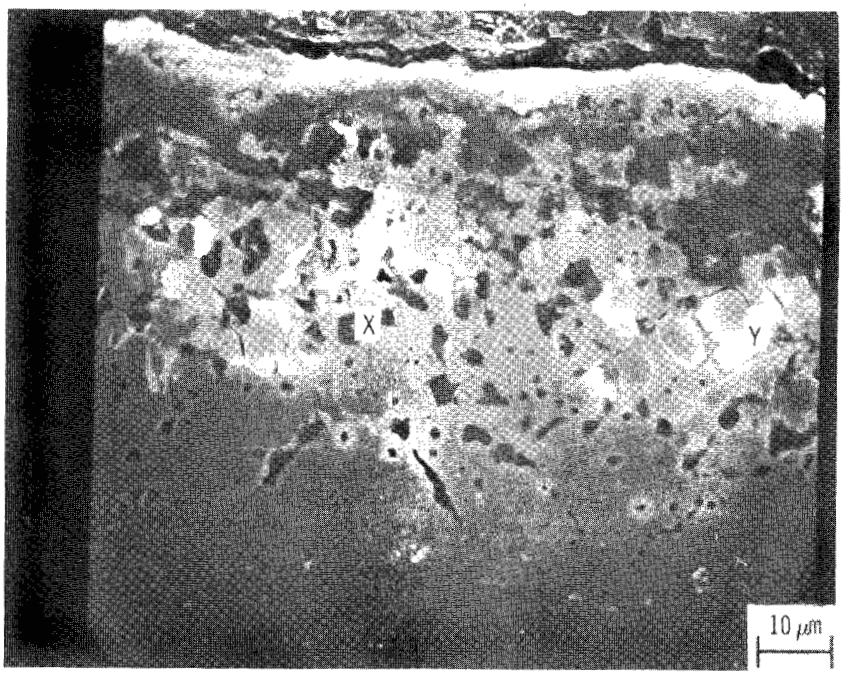

(a) Microstructure.

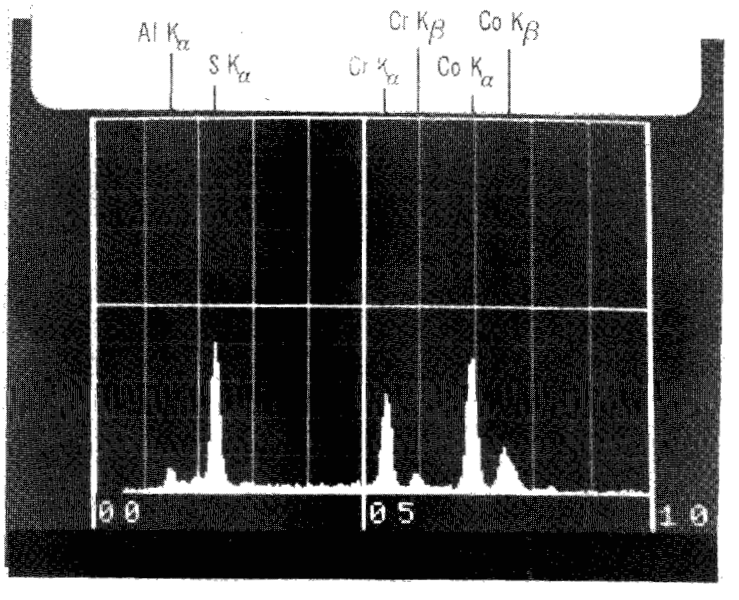

(b) Energy dispersive spectrum of dark particle marked X in part (a). X30 000.

Figure 12. - Microstructure and energy dispersive spectrums of internal corrosion zone of S-57 corroded at 900° C with 4 ppm sodium sulfate.

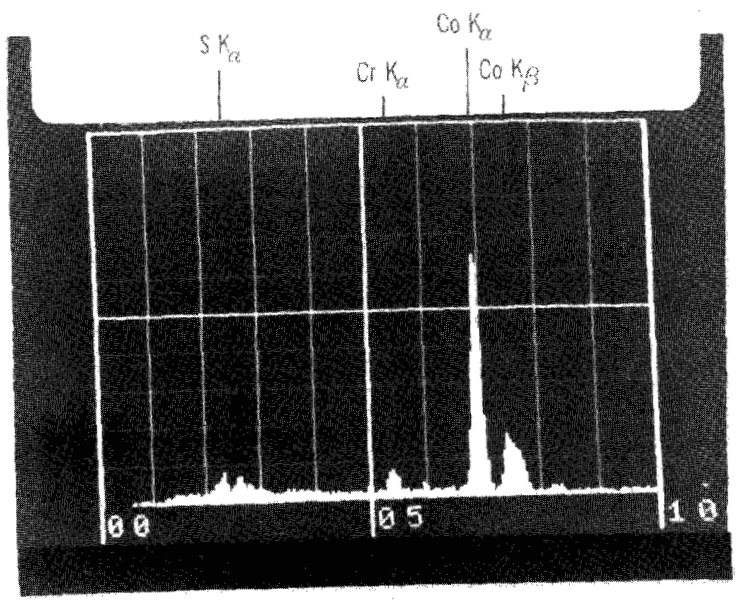

(c) Energy dispersive spectrum of light area marked Y in part (a). X10 000.

Figure 12. - Concluded.

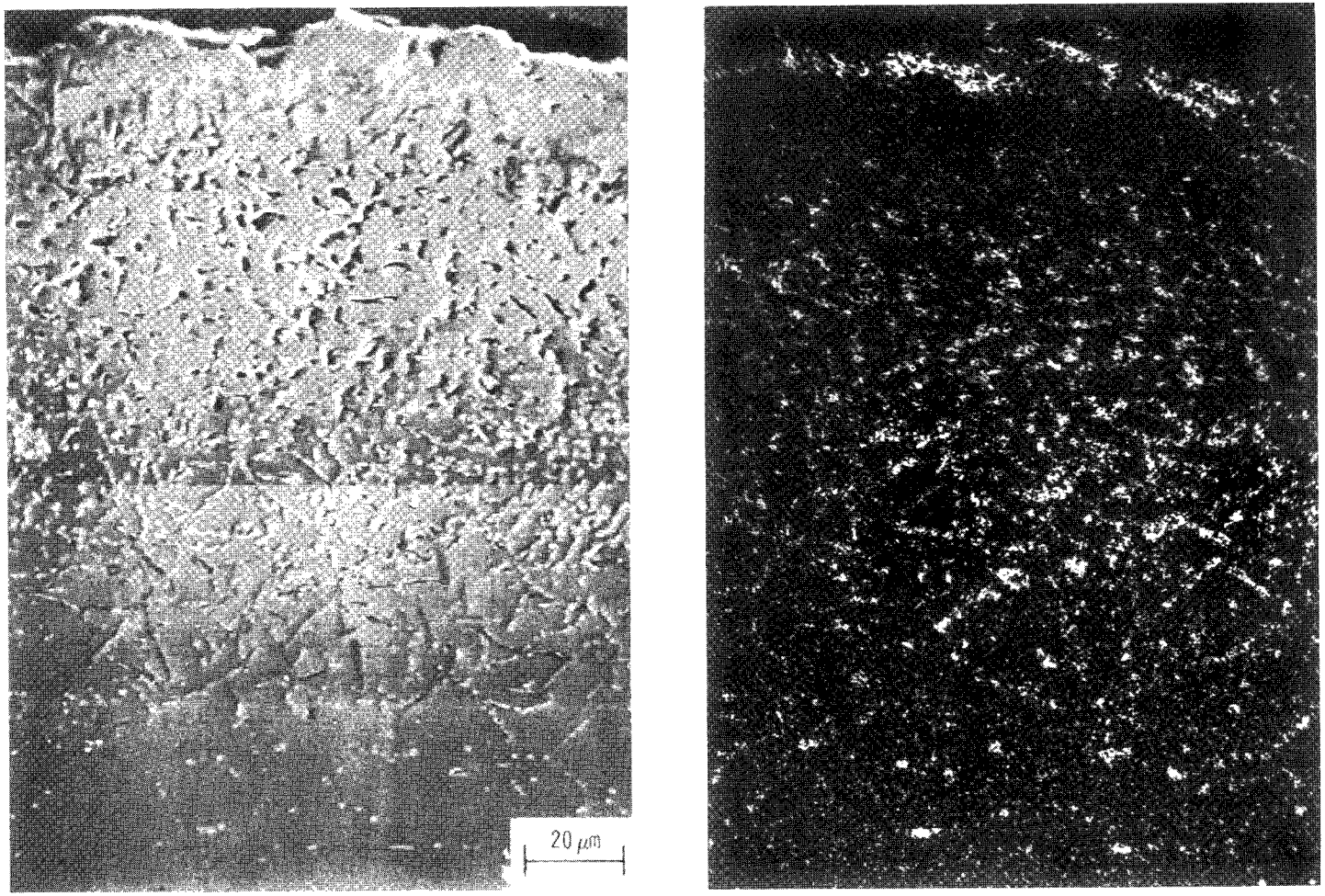

(a) Secondary electron image.

(b) Tantalum M_α raster scan.

Figure 13. - Secondary electron image and raster scans showing tantalum enrichment at interface of scale and internal corrosion zone and both tantalum and aluminum enrichment in internal corrosion zone of S-57 corroded at 1000° C with 10 ppm sea salt.

(c) Aluminum K_{α} raster scan.

Figure 13. - Concluded.

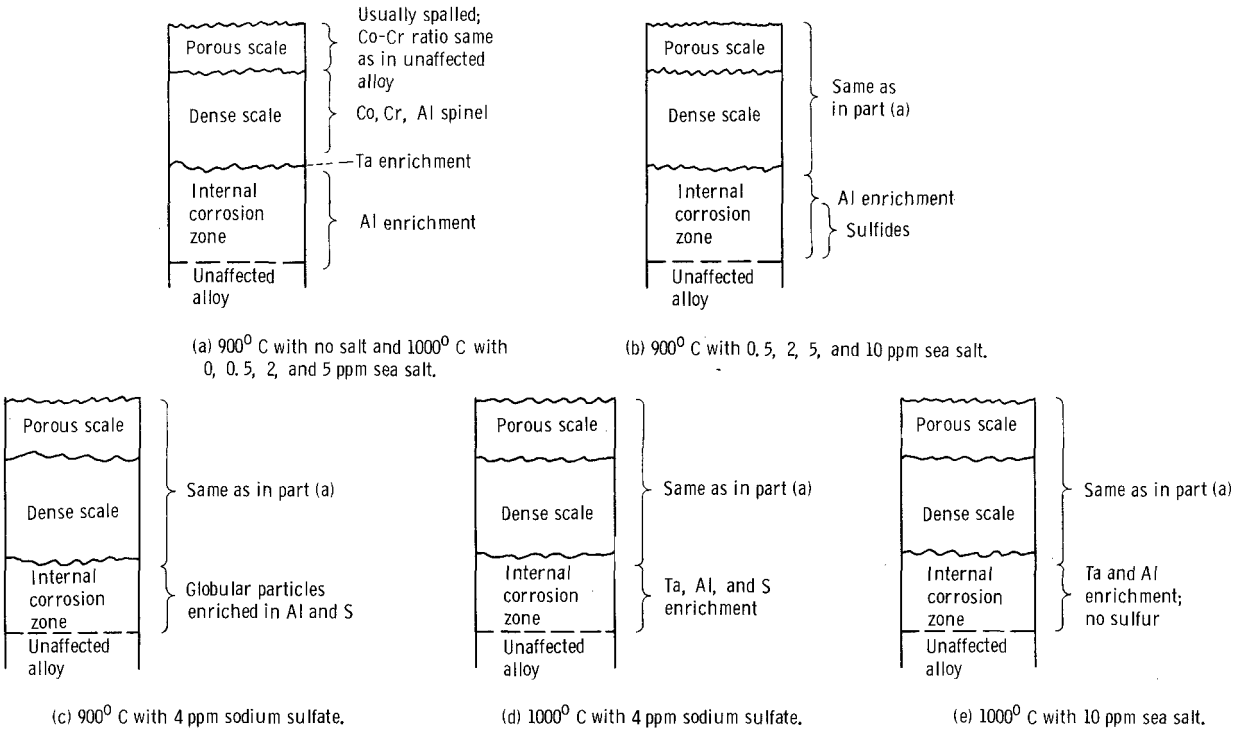

(a) 900° C with no salt and 1000° C with 0, 0.5, 2, and 5 ppm sea salt.

(b) 900° C with 0.5, 2, 5, and 10 ppm sea salt.

(c) 900° C with 4 ppm sodium sulfate.

(d) 1000° C with 4 ppm sodium sulfate.

(e) 1000° C with 10 ppm sea salt.

Figure 14. - Schematic representations of microstructures of S-57 corroded at various conditions.

"The aeronautical and space activities of the United States shall be conducted so as to contribute . . . to the expansion of human knowledge of phenomena in the atmosphere and space. The Administration shall provide for the widest practicable and appropriate dissemination of information concerning its activities and the results thereof."

—NATIONAL AERONAUTICS AND SPACE ACT OF 1958

NASA SCIENTIFIC AND TECHNICAL PUBLICATIONS

TECHNICAL REPORTS: Scientific and technical information considered important, complete, and a lasting contribution to existing knowledge.

TECHNICAL NOTES: Information less broad in scope but nevertheless of importance as a contribution to existing knowledge.

TECHNICAL MEMORANDUMS: Information receiving limited distribution because of preliminary data, security classification, or other reasons. Also includes conference proceedings with either limited or unlimited distribution.

CONTRACTOR REPORTS: Scientific and technical information generated under a NASA contract or grant and considered an important contribution to existing knowledge.

TECHNICAL TRANSLATIONS: Information published in a foreign language considered to merit NASA distribution in English.

SPECIAL PUBLICATIONS: Information derived from or of value to NASA activities. Publications include final reports of major projects, monographs, data compilations, handbooks, sourcebooks, and special bibliographies.

TECHNOLOGY UTILIZATION PUBLICATIONS: Information on technology used by NASA that may be of particular interest in commercial and other non-aerospace applications. Publications include Tech Briefs, Technology Utilization Reports and Technology Surveys.

Details on the availability of these publications may be obtained from:

SCIENTIFIC AND TECHNICAL INFORMATION OFFICE

NATIONAL AERONAUTICS AND SPACE ADMINISTRATION

Washington, D.C. 20546